Electromagnetic characterization of a big aperture magnet used in particle beam cancer – (ECBAMUPBC)

Jhonnatan Osorio*[1], Cristiana Priano[2], Marco Pullia[3]
[1]CNAO foundation, [2]CNAO foundation, [3]CNAO foundation
*Jhonnatan.moreno@cnao.it, Strada Campeggi 53 Pavia-Italy

Abstract: After validation of COMSOL simulations with measurements of a CNAO synchrotron dipole, COMSOL Multiphysics has been used to evaluate the magnetic field quality of the CNAO large gap 90° bending magnet. A stiffening frame and welded tie bars are employed to provide the mechanical rigidity of the magnet and their impact on the field quality has been investigated. Simulations show an increment of 0.82% in the magnetic field strength due to the structural elements, but this effect does not affect the magnetic field homogeneity. 2D dynamic simulations have been performed and have shown a field decay with time constant of 1.13 s. The ramp used for this magnet is sufficiently slow that the transitory effects vanish while the beam is accelerated, such that when the beam is extracted the magnetic field is already stable.

Keywords: Hadrontherapy**,** Magnetic field quality, 90° bending magnet, Carbon Ions.

1. Introduction

Resistive magnets are one of the main components of synchrotrons used in particle therapy. A particular large aperture magnet has been installed in the Centro Nazionale di Adroterapia Oncologica (CNAO), which is a synchrotron accelerator facility dedicated to cancer treatment with protons and carbon ions.

This magnet is used in one of the CNAO extraction lines to bend the beam by 90° and direct it vertically onto the patient. A layout of the treatment line where the magnet is installed is shown in figure 1. The dipole has to generate magnetic fields up to 1.81 T in a region of 20 x 20 cm^2 along the beam path.

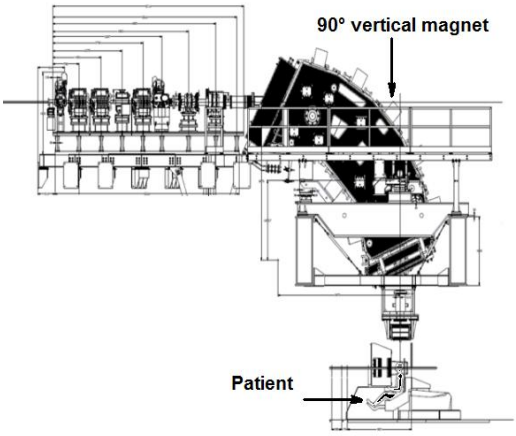

Figure 1 Schematic layout of CNAO vertical line.

To preserve the beam quality, the relative variations in field strength inside the 20 x 20 cm^2 region where the beam passes should be less than $2x10^{-4}$. This region is called the Good Field Region (**GFR**). The observed quantity is the field homogeneity

$$\frac{\Delta B}{B} = \frac{B(x,y) - B_0(x,y)}{B_0(x,y)} \qquad (1)$$

This article shows the 2D static and dynamic calculations of the 90° CNAO bending magnet using the AC/DC COMSOL module where the equation that characterizes the phenomena is the Ampere's law in a material medium.

$$\nabla \times H(\vec{r},t) = j(\vec{r},t)$$
$$\mu\vec{H} = \nabla \times \vec{A}$$

2. 90° bending magnet specifications

The basic specifications for the magnet considered are listed in table 1.

Table 1: Technical specifications of the 90° CNAO bending magnet [1].

Parameter	Value
Nominal field [T]	1.81
Ramp rate [T/s]	0.4
Bending radius [mm]	3650
Edge angle (upstream) [deg]	30
Edge angle (downstream) [deg]	21
Good Field Region (GFR) around ref trajectory [mm x mm]	±100 x ±100
Turns per pole	80
Nominal current [A]	2280
Maximum magnet weight [t]	75
Integrated field quality [ΔBL/BL]	$\leq \pm 2 \times 10^{-4}$

The magnet is a window frame type with two saddle coils. The average current density carried by the coils is 4.056×10^6 A/m^2. Figure 2 shows the main dimensions of the magnet.

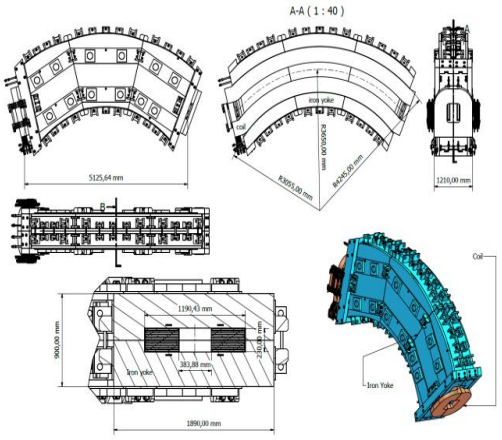

Figure 2. Main details of the 90° CNAO bending magnet.

Since the magnet has to be ramped in times of the order of 5 s, the iron yoke has to be laminated; this magnet has been built with 1 mm thick laminations made of EBG 1200-100A iron.

3.0 COMSOL calculations

The dynamic behavior of the CNAO 90° bending magnet has not been measured during the construction phase because the constructing firm did not have a suitable power supply. Measured data therefore not available to compare and validate the COMSOL calculations.
To validate the simulations, an initial test has been done comparing the measurements performed on the main synchrotron CNAO dipole and a 2D COMSOL simulation of the same magnet. Its main characteristics are: 1.5 T nominal magnetic field, 120x56 mm^2 GFR. Tension bars similar to the ones used in the 90° dipole are used to provide the mechanical stability of the magnet [2].

Measurements of the magnet show that a part of the field lags with a time constant of the order of 0.5-1 s. Figure 3 shows measurement and simulation of the field stabilization.

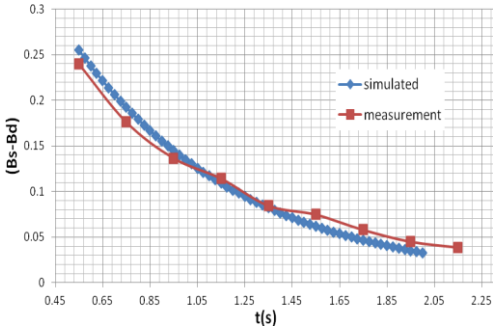

Figure 3. Difference between static field (Bs) and dynamic field (Bd) at the end of the feeding current ramp. Measurement and calculated data are show

The time needed for the field to be considered stable, depends on how accurate the values has to be. Considering acceptable, as an example, variations of 0.1% between the stationary reference field 1.539 T, (plateau region shown by the red line in figure 4) and the dynamic field values (blue line figure 4) the calculated stabilization time for the synchrotron dipole magnet is 681 ms after the ramp ends. The measured time for this magnet was 650 ms.

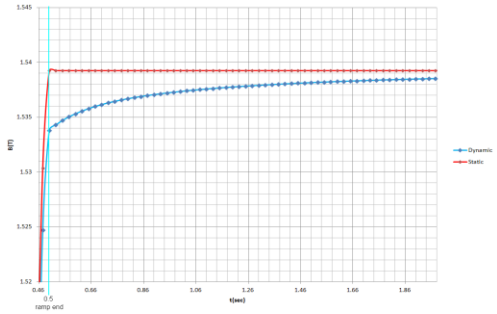

Figure 4. Magnetic field strength calculated in the center of the synchrotron magnet using a parametric feeding current sweep (red line) and a time dependent solver (blue line). The feeding current ramp used is 5630 A/s.

This result shows a good agreement between the experimental results and the calculations performed by COMSOL.

3.1 Characterization of the 90° CNAO bending magnet

Static regime simulations have been performed at the nominal current of 2280A; the influence of the stiffening frame and the tension bars on the magnetic field strength in the center of the magnet has been evaluated. Figure 5 shows the CAD model

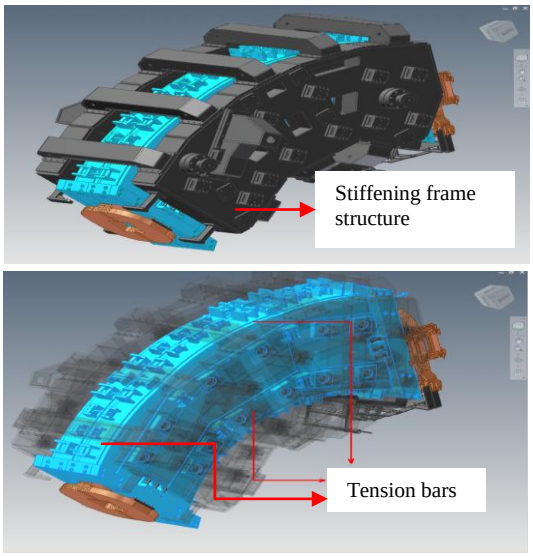

Figure 5. CAD model of the 90° CNAO bending magnet, exploiting the magnet symmetry, half magnet. has been simulated.

Figure 6 shows the 2D simplified geometry used in COMSOL.

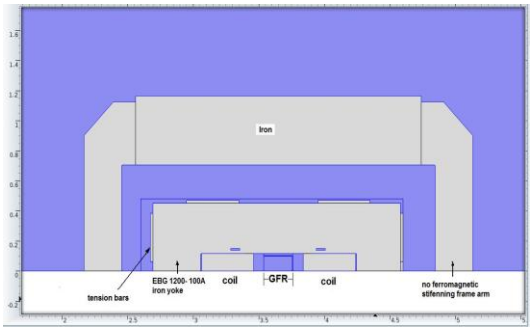

Figure 6. 2D model simplification used in COMSOL

The 2D simplified 90° bending magnet model evaluates some important aspects, in particular:

- the magnetic field homogeneity in the GFR;
- the effect on the magnetic field strength of additional iron structural elements that help in the mechanical magnet stability;
- the saturation effects on the iron yoke.

To assess the field quality inside the good field region, the magnetic field has been calculated at 11 different heights, one cm apart from each other, above the symmetry plane. Figure 7 shows schematically the lines along which the field homogeneity was evaluated and figure 8 reports the relative results.

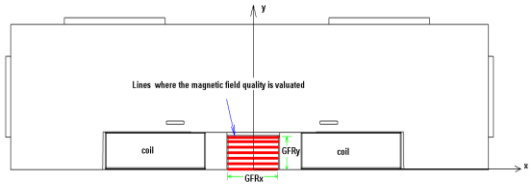

Figure 7**.** Sketch of horizontal lines used to evaluate the magnetic field and its homogeneity.

2D static simulation (figure 8) shows that the field value inside the iron yoke is near to the saturation level of 1.8 T reported for the EBG 1200-100A iron yoke material [1]. However, this magnet has been designed to work up to the saturation limit in order to minimize the amount of iron. The calculated magnetic field intensity is 1.8759 T (see figure 8) and the magnetic field homogeneity along the horizontal lines described in figure 7 is better than ± 2.8 x 10^{-4} for the entire GFR (see figure 9).

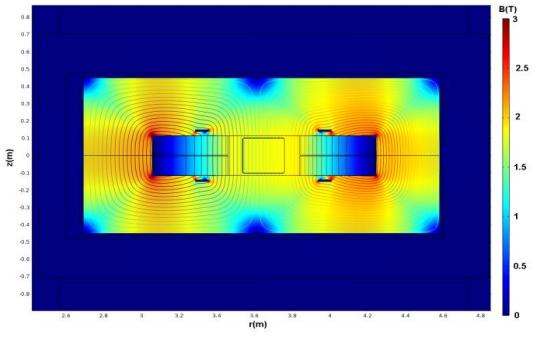

Figure 8. Magnetic flux density of the 90° bending magnet

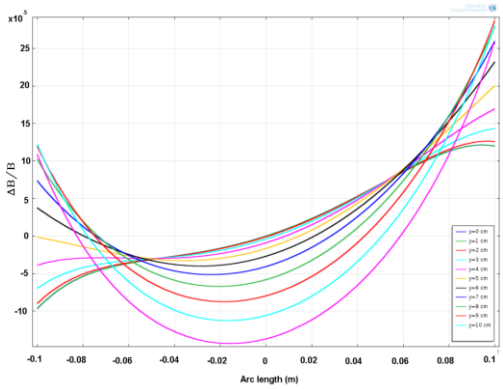

Figure 9. Magnetic field quality in the GFR. The plotted values in the field quality are relative to equation (1).

The simulated field quality slightly exceeds the specification (see table 1), however the relevant field quality is the integrated field quality which can be evaluated exclusively by a 3D model. Although the 2D homogeneity is out of the specification, the maximum - minimum value calculated in the GFR is approximately $4x10^{-4}$, which is the same extent as $\pm$ 2 x 10^{-4}.

The tension bars and the stiffening frame have an influence on the field in the GFR also in the 2D static regime calculation. This is more evident for the tension bars, which are directly welded on the iron yoke. The resulting increment in the magnetic field is due to the reduction of the magnetic circuit reluctance. The effect is non-negligible, with an increment of about the 0.82% in the magnetic field strength in the gap for the tension bars; the contribution of the stiffening frame is smaller and accounts for a variation of 0.1%. The effects of the different elements on the magnetic field are summarized in table 2.

Table 2: Values of the magnetic field strength in the middle of the GFR

	B in the center of the magnet [T]	**Delta (%)**
Only iron yoke	1.8759	0
Yoke+tension bars	1.8913	0.82
Yoke+ tension bars + stiffening frame	1.8932	0.92

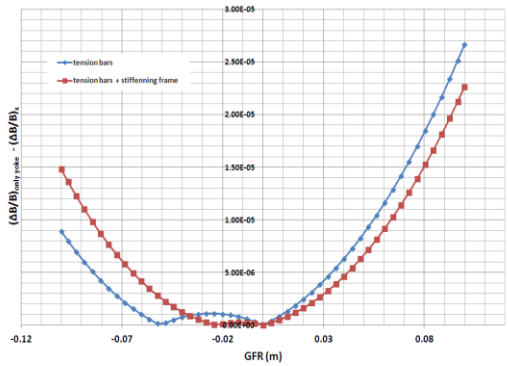

Figure 10: Differences between the field homogeneity of iron yoke and yoke+tension bars and yoke+tension bars+ stiffening frame.

Although the differences between the field intensity are not negligible when are considering the stiffening frame and the tension bars, the impact of these additional elements in the field homogeneity can be neglected, the variations are below $2.5x10^{-5}$ (see figure 10).

3.2 Dynamic behavior of the 90° CNAO bending magnet

As it has been shown previously in this section, external structural elements, like the tension bars, contribute to a time delay in reaching the operational point of the magnet. In the CNAO 90° bending magnet, 8 tension bars were welded along the yoke and they are used to place additional elements needed to connect the magnet to the stiffening frame (see figure 5).

To build a 2D model of a 3D predominant physics effect it is necessary to consider several simplifications; the specific assumptions in the model are the following:

- The 2D profile represents a perfect lamination of the iron yoke, there is no propagation of the magnetic flux lines along the beam axis.
- The excitation current ramp is shown in fig 11 and reaches a maximum of 2124 A in 4.5 s.
- The tension bars were simulated with the same B-H curve of the iron yoke and an electric conductivity of $2.5x10^{6}$ S/m.

As shown in fig 5, the stiffening frame is composed by two plates connected by lateral beams. In this simulation the structure was considered as a solid iron slab on the upper part of the yoke and the lateral arms were considered non-magnetic (figure 6).

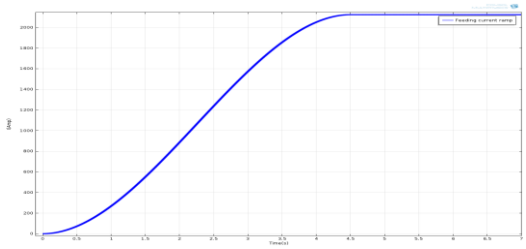

Figure 11: excitation current versus time used in the dynamic calculations of the 90 bending CNAO magnet.

Figure 12 illustrates the eddy currents in the tension bars in two different instants of the magnetic ramp. The magnetic field has the behavior expected: the magnetic flux lines do not penetrate into the tension bars in the initial phase of the current ramp (t = 0.25 s) and they begin to enter at the end of the ramp.

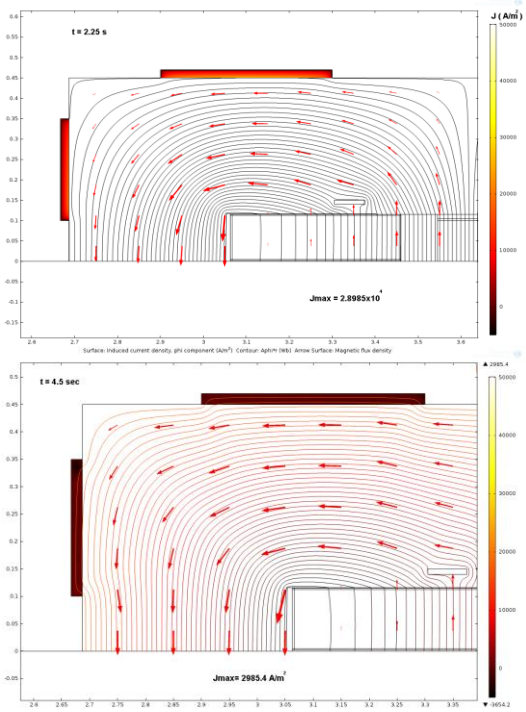

Figure 12: Magnetic flux lines and eddy current distribution in the tension bars at 2.25 sec and at the end of the ramp (4.5 sec).

The mechanism behind the field stabilization time effect can be described by the Lenz's effect generated in the tension bars, which prevent the magnetic flux penetrating this region (fig 12). After the ramp end, the eddy currents decay and the magnetic flux can use the tension bars as an additional path. This reduces the reluctance of the magnetic circuit, resulting in a field increase in the air gap of the GFR, as it has been shown in the static simulation. A plot of the difference between static and dynamic regime puts in evidence the entire effect along the flat top, when the excitation current is constant (fig 13).

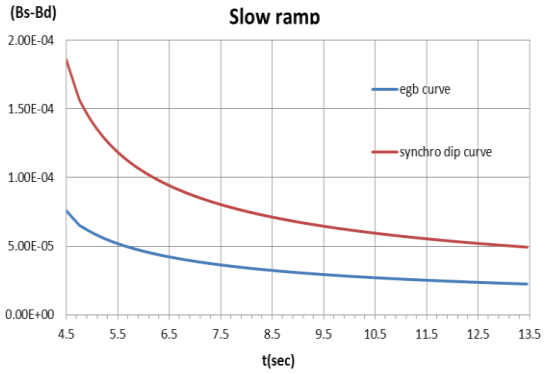

Figure 13: Difference between static field (Bs) and dynamic field (Bd) at the end of the feeding current ramp (t=4.5 s. in figure 11) for two different yoke materials.

This representation permits to evaluate the "decay time" of the eddy currents. The curves shown in figure 13 have been fitted with the sum of two exponential functions:

$$f(t) = Ae^{\left(\frac{t-t_0}{t_a}\right)} + Be^{\left(\frac{t-t_0}{t_b}\right)} \quad (2)$$

where t_0 =4.5s is the moment when the ramp ends. The two decay constants t_a and t_b are 1.13 an 13.3 s respectively. However, for the purpose of this magnet, the delay time effect can be neglected, because the differences between the magnetic field strengths (Bs-Bd) are below 10^{-4} T (fig 13). This negligible delay time effect can be explained by the low ramp rate. In the tension bars it generates small eddy currents such that they vanish almost completely before the end of the ramp.

With the bias of the previous experience of the synchrotron dipoles, the amount of lagging field in the 90° magnet was surprisingly small. The reason for such a small effect could be either in the different BH curve and/or in the lower ramp rate.

The simulation was therefore repeated with the two different materials (the one of the extraction lines and the one of the synchrotron) and two different ramp rates. The first one is referred to as "**fast ramp**", which means a ramp of 4248 Amp/s (the operational current is reached at 0.5 sec) and represents the case when the 90° magnet is ramped like a synchrotron dipole. The second case is called "**slow ramp**", which means a ramp of 503.8 Amp/s and represents the nominal operational conditions of the 90° magnet (figure 13).

The "Synchro dip curve" in figures 13 and 14 represents the simulation performed with the iron yoke material properties equal to the B-H curve of a synchrotron dipole magnet and the "egb curve" represents the behavior with the EBG iron yoke material.

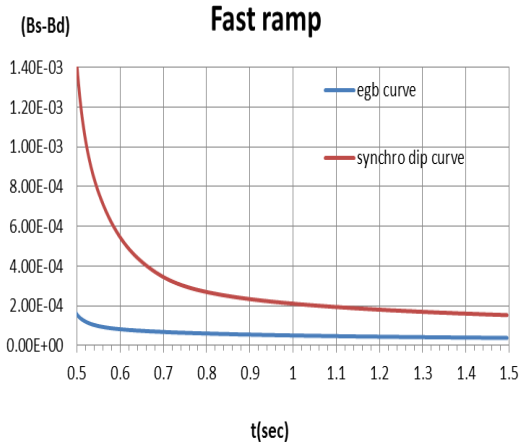

Figure 14: Difference between static field (Bs) and dynamic field (Bd) at the end of the synchrotron feeding current ramp (t=0.5 s and dI/dt=4248 A/s) for two different yoke materials.

Figures 13 and 14 show the Cockerill steel of the synchrotron dipoles yields a larger amount of lagging field with respect to the EBG. As expected, the fast ramp generates larger differences between the dynamic and the static magnetic fields compared to the slow ramp case.

A 90° dipole similar to the one described here, with an improved stiffening frame, is considered in the conceptual design of a carbon ion gantry [3],[4]. The magnet design study is in progress.

A gantry is a rotating transfer line that allows patient irradiation from any directions. A layout of such possible application for the big aperture magnet is shown in figure 15.

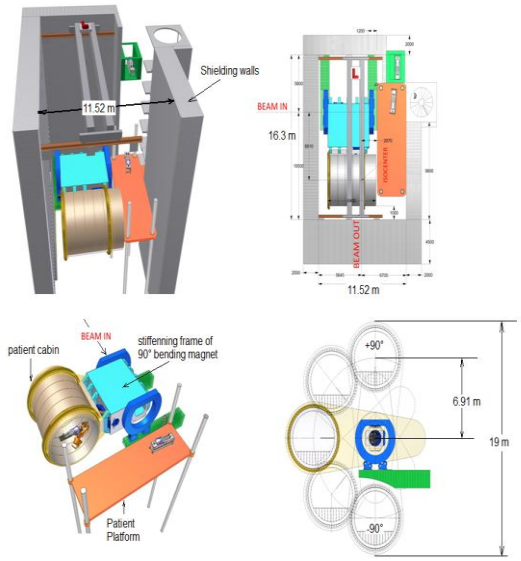

Figure 15 Perspective and plant view of the mobile isocenter gantry with the building housing it. On the bottom, two sketches of the main gantry structural elements and an example of the ± 90° treatment cabin rotation [4].

4. Conclusions

Static simulations of the CNAO 90° large gap dipole have shown that the 2D field homogeneity is acceptable and that influence of the stiffening structure and of the tension bars cannot be neglected.

The variation in the absolute value of the field in the gap is not significant in the requirement on the excitation current (it even improves the situation) and the effect on the field homogeneity is unimportant.

On the other hand the field variation due to the tie bars and to the stiffening frame grows with a time constant depending on the eddy currents inside them; such time constants are non negligible on the time scale of the machine operation. Anyway, comparison of static and dynamic simulations of the CNAO 90° large gap dipole have shown that, because of the low ramp rate and of the good behavior of the EBG iron, the magnet can be operated without significant field lag at the nominal ramp rate.

5. References

1. C.Priano, M.Pullia, P.Fabricattore , *Magnetic design improvement and construction of the large 90° bending magnet of the vertical beam delivery line of CNAO*, 1782-1784. Proceedings of EPAC, Genova (2008)

2. T. Zickler, *Design and optimization of the medaustron synchreotron main dipoles*, Proceedings of IPAC, San Sebastian, Spain (2011)

3. J.Osorio, *WP21–D3 Final report of the project of a novel carbon ion gantry design*, internal communication PARTNER project (2012) website:http://partner.web.cern.ch/partner/cms/?file=home

4. V. Lante, M.M. Necchi, S. Savazzi, J. Osorio Moreno, *Deliverable Report JRA6.2– conceptual design of the gantry explaining the choices made.* Internal communication ULICE project (2012).

6. Acknowledgements

This study has been done thanks to fundings from the European Community in the Seventh Frame Work Program, 2007-2012 PARTNER Project, under agreement n° 215840-2.